




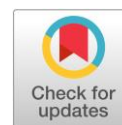
## Features of forming a cubic $\text{Li}_7\text{La}_3\text{Zr}_2\text{O}_{12}$ film by tape casting

Efim Lyalin<sup>a\*</sup> , Larisa Pershina<sup>b</sup>, Evgeniya Il'ina<sup>a</sup> ,  
Konstantin Druzhinin<sup>a</sup> , Semen Belyakov<sup>a</sup> 

**a:** Laboratory of Electrochemical Power Sources, Institute of High Temperature Electrochemistry, Ural Branch of the Russian Academy of Sciences, Ekaterinburg 620990, Russia

**b:** Department of Building Materials Science, Institute of New Materials and Technologies, Ural Federal University, Ekaterinburg 620009, Russia

\* Corresponding author: [efim.lyalin.2013@inbox.ru](mailto:efim.lyalin.2013@inbox.ru)



This paper belongs to a Regular Issue.

### Abstract

Currently, interest to lithium and lithium-ion all-solid-state power sources is rapidly growing all over the world. However, several issues should be addressed before all-solid-state batteries production: high resistance values of the solid electrolyte membrane and poor contact between electrolyte and electrode materials. The transition to thin-film technologies is one of the promising ways to solve these problems. Tape casting can be proposed to obtain thin-film solid electrolytes. In this research, the features of the structure formation, morphology and lithium-ion conductivity of  $\text{Li}_7\text{La}_3\text{Zr}_2\text{O}_{12}$  films were investigated.  $\text{Li}_7\text{La}_3\text{Zr}_2\text{O}_{12}$  films with the thickness of 35  $\mu\text{m}$  were obtained by tape casting on Ni substrate. The influence of organic components' content on homogeneous coatings formation was established. Heat treatment conditions for dried films were chosen based on differential scanning calorimetry and optical dilatometry. Phase change from tetragonal to cubic modification occurs after annealing the  $\text{Li}_7\text{La}_3\text{Zr}_2\text{O}_{12}$  films at 700 °C and higher. The annealed  $\text{Li}_7\text{La}_3\text{Zr}_2\text{O}_{12}$  films have developed surface, which can lead to improved contact between the solid electrolyte and an electrode in an electrochemical cell.  $\text{Li}_7\text{La}_3\text{Zr}_2\text{O}_{12}$  films annealed at 800 °C have the highest lithium-ion conductivity values ( $2.5 \cdot 10^{-7}$  and  $1.5 \cdot 10^{-5}$   $\text{S} \cdot \text{cm}^{-1}$  at 90 and 215 °C, respectively). The technology of  $\text{Li}_7\text{La}_3\text{Zr}_2\text{O}_{12}$  films formation with the thickness of  $\sim 23$   $\mu\text{m}$  by tape casting was developed.

### Key findings

- Thin films of  $\text{Li}_7\text{La}_3\text{Zr}_2\text{O}_{12}$  solid electrolyte were obtained by tape casting.
- The optimal heat treatment mode without films' deformation was proposed.
- The highest conductivity values were observed for the  $\text{Li}_7\text{La}_3\text{Zr}_2\text{O}_{12}$  film annealed at 800 °C –  $1.5 \cdot 10^{-5}$   $\text{S} \cdot \text{cm}^{-1}$  at 215 °C.

### Keywords

$\text{Li}_7\text{La}_3\text{Zr}_2\text{O}_{12}$   
lithium-ion conductivity  
film  
tape casting  
all-solid-state battery

Received: 13.10.23

Revised: 07.11.23

Accepted: 17.11.23

Available online: 21.11.23

© 2023, the Authors. This article is published in open access under the terms and conditions of the Creative Commons Attribution (CC BY) license (<http://creativecommons.org/licenses/by/4.0/>).

## 1. Introduction

Lithium power sources are in great demand in the modern world. Currently, interest to lithium-ion and lithium all-solid-state batteries (ASSB) is growing, because such power sources possess stability at high temperatures, long life and safety [1, 2]. Medium-temperature (up to 300 °C) batteries

for special applications operating in extreme conditions can be created by transition from traditional lithium-ion batteries to ASSB. In turn, transition to film structures in such power sources opens up new opportunities for miniaturization and material cost reduction in mass production. Moreover, electrolytic membrane thickness plays a crucial role in the electrochemical performance of ASSB [3]. Thus, the

development and use of solid electrolyte films and electrochemical devices based on them has a great potential for various applications and is one of the most important tasks of modern science and technology.

$\text{Li}_7\text{La}_3\text{Zr}_2\text{O}_{12}$  (LLZ) is one of the most promising lithium-ion solid electrolytes for depositing films due to its electrochemical and physical properties. It is known that undoped LLZ has two modifications: cubic and tetragonal. According to the literature [4–8], transition from tetragonal to cubic modification occurs in the range from 350 to 800 °C at various heat treatment conditions. Both modifications have conductivity values of  $10^{-6}$ – $10^{-7}$  S·cm<sup>-1</sup> at 25 °C. However, addition of some doping element leads to stabilization of highly conductive cubic structure of LLZ ( $10^{-4}$  S·cm<sup>-1</sup> at 25 °C). Combination of stability in contact with lithium metal and high ionic conductivity makes  $\text{Li}_7\text{La}_3\text{Zr}_2\text{O}_{12}$  a very attractive material for ASSB [9–11]. However, the presence of mechanical defects and impurity phases can significantly reduce conductivity of the thin-film electrolyte and thereby worsen the electrochemical properties of assembled battery. To solve this problem, some methods for obtaining single-phase homogeneous films of solid electrolyte should be developed.

In the literature [12–21], different methods for obtaining LLZ films are presented. For example, physical methods include techniques based on evaporation or target spraying. Thin-films hundreds of nanometers thick can be obtained by spraying or vaporizing a target in vacuum [12, 13]. For example, J. Tan and A. Tiwari successfully produced LLZ thin films by pulsed laser deposition, which is based on target evaporation [13]. The freshly deposited films had an amorphous structure with a thickness of ~1 μm and showed an ionic conductivity of  $3.35 \cdot 10^{-7}$  S·cm<sup>-1</sup> at room temperature. Their annealing at 800 °C led to the cubic modification formation and conductivity growth up to  $7.36 \cdot 10^{-7}$  S·cm<sup>-1</sup> at room temperature. Chemical methods are also widely used for the film deposition [14, 15]. Films with the thickness of several tens to hundreds of nanometers can be formed by dip-coating and spin-coating. However, this requires preparing a precursor of a certain concentration. K. Tadanaga et al. [14] developed the solid electrolyte precursor in the form of solution for dip-coating technique.  $\text{LiNO}_3:\text{La}(\text{NO}_3)_3 \cdot 6\text{H}_2\text{O}:\text{Zr}(\text{O}-\text{n}-\text{C}_3\text{H}_7)_4:\text{Al}(\text{O}-\text{sec}-\text{C}_4\text{H}_9)_3:\text{EAcAc}:1\text{-propanol}$  were mixed in molar ratio 7.7:3.0:2.0:0.3:4.0:50, respectively. The obtained coatings also had the amorphous structure and the thickness of 1 μm. The cubic modification of LLZ was obtained with a small amount of  $\text{LaAlO}_3$  impurity after heat treatment at 900 °C.

It should be noted that these techniques are difficult to implement due to expensive equipment and complex technical process. The obtained films have amorphous structure and require additional heat treatment to form the necessary structure. Unlike these techniques, electrochemical methods and ceramic technologies use solid electrolyte with the already formed phase. The deposited coatings are com-

pletely identical with the powder of initial material. For example, we have recently shown that the electrophoretic deposition method is a promising technique for producing thin-film solid electrolytes based on LLZ [16]. LLZ films with tetragonal modification and a thickness of 25 μm were obtained on a Ti substrate.

Tape casting is one of the most widely used methods for producing ceramic materials in the form of thin films or sheets. This technique has significant advantages due to the scalability and continuity of tape casting process. However, the slurry composition must be carefully developed. According to the literature [17–19], fish oil (dispersant), polyvinyl butyral (binder), butylbenzyl phthalate or polyethylene glycol (plasticizer) are the most popular components of the slurry. Toluene, ethanol or isopropanol are used as solvent. For example, E. Yi et al [17] obtained a thin-film coating of cubic  $\text{Li}_{6.25}\text{Ga}_{0.25}\text{La}_3\text{Zr}_2\text{O}_{12}$ . The suspension was prepared on the basis of ethanol + acetone system by mixing solid electrolyte powder with polyacrylic acid dispersant, polyvinyl butyral binder and butylbenzyl phthalate plasticizer. After removal of organic components by heat treatment at 1130 °C for 0.3 h, membrane thickness was equal to 25 μm, and conductivity reached  $1.3 \cdot 10^{-3}$  S·cm<sup>-1</sup> at room temperature. R. Ye et al [20] developed a more environmentally friendly slurry. They used environmentally friendly components: methylcellulose binder and mixture of plasticizers (polyethylene glycol + glycerol), which were dissolved in distilled water. The samples obtained after heat treatment demonstrated a total ionic conductivity of  $1.5 \cdot 10^{-4}$  S·cm<sup>-1</sup> at room temperature.

It should be noted that in the literature only the studies on doped LLZ films have been reported. It is well known that stabilization of highly conductive cubic modification requires the addition of some dopant (for example, Ga, Ta, ...) [21], which lead to the complication of production process. However, the conductivity values of doped and undoped LLZ become comparable at 300 °C [21]. So, transition to undoped  $\text{Li}_7\text{La}_3\text{Zr}_2\text{O}_{12}$  for use in medium-temperature ASSB can significantly reduce the cost of device manufacturing. No complete study linking the parameters of technological mode and postforming of LLZ solid electrolyte film of tetragonal modification with its functional characteristics has been presented in the literature.

The aim of our work is to study the features of structure formation, morphology and conductivity of thin-film LLZ solid electrolyte obtained by tape casting.

## 2. Materials and Methods

To prepare a slurry, solid electrolyte powder of LLZ was synthesized by citrate-nitrate method. The slurry was obtained by grinding a mixture of the starting components in a ball mill (FRITSCH, Germany). The slurry components were chosen based on the patent [22]:  $\text{Li}_7\text{La}_3\text{Zr}_2\text{O}_{12}$ ; polyvinyl butyral (binder); polyethylene glycol (plasticizer); fish oil (dispersant); isopropanol. The mass ratio of grinding

balls to the slurry was 3 to 1, respectively. The grinding mode was empirically chosen. The slurry was well homogenized and did not overheat at 450 rpm for 24 h. Degassing was carried out without grinding balls at 200 rpm for 5 h. After degassing, the slurry was cast by a doctor blade on a nickel substrate. Then obtained film was dried at 45 °C for 1 h.

The conditions of organic components removal from the film composition was determined by simultaneous thermal analysis (STA). STA measurements were performed using a thermal analyzer STA 449C Jupiter (Netzsch, Selb, Germany). The experiments were carried out in Pt pans in the temperature range of 35–900 °C with a heating rate of 10 °C·min<sup>-1</sup> in air (20 mL·min<sup>-1</sup>). The obtained data were processed by a NETZSCH Proteus software. The heating rate was optimized using optical dilatometry on an ODP 868 device (TA Instruments, USA) in the temperature range from 25 to 900 °C with different heating rates: 2 and 5 °C·min<sup>-1</sup>. A 30×2 mm film sample was placed on an yttria-stabilized zirconia substrate. The transverse profile of the film was observed in the heating microscopy mode.

The heat treatment was carried out in three subsequent stages:

- 1) heating from room temperature to 200 °C (1 °C·min<sup>-1</sup>) and exposure at 200 °C for 1 h;
- 2) heating from 200 to 500 (5 °C·min<sup>-1</sup>) and exposure at 500 °C for 30 min;
- 3) heating from 500 to a final annealing temperature (600, 700, 800 or 900 °C) with the 5 °C·min<sup>-1</sup> heating rate and exposure for 30 min. LLZ coatings on Ni substrates were annealed in argon atmosphere using a high-temperature tube furnace SOUL 2/14-V (SOUL, Russia).

The densities of the studied samples were determined by hydrostatic weighing based on Archimedes' principle using gasoline with a density of 0.7 g·cm<sup>-3</sup>.

XRD analysis of LLZ powder and films annealed at different temperatures was carried out using a Rigaku D-MAX-2200 V diffractometer (Rigaku, Tokyo, Japan) with a vertical goniometer and Cu K-radiation, 2θ = 10–55°. XRD patterns of compounds were compared with the database (ICDD PDF-2) and the literature data [23–25].

Scanning electron microscopy (SEM) study of the samples' surface was carried out using a MIRA3 FEG SEM (Tescan, Brno-Kohoutovice, Czech Republic) in backscattered electron (BSE) and secondary electron (SE) modes. The element distribution investigation was performed using JEOL JSM 5900LV Scanning Electron Microscope with Oxford Instruments INCA Energy Dispersive Spectrometer (Richland, USA). The films' cross-sections were studied using an AmScope 3.0 optical microscope (AmScope, UK). The films deposited on Ni substrate were placed in a container and filled with epoxy resin and hardener (Epoxy glue EXPERT, Russia) in a ratio of 4:1, respectively. After hardening, the cross section surface was leveled using a grinding wheel with a diamond abrasive grit of 200/160 μm. The final polishing of the samples was carried out using

sandpaper with grits (P) 3000 and 5000. The polished cross section surface was cleaned with isopropanol.

Resistances of the obtained films (initial and annealed at 600, 700, and 800 °C) were determined by electrochemical impedance spectroscopy using an E7-25 immittance meter (MNIPI, Minsk, Belarus) in the frequency range of 0.025–1000 kHz. Gallium-silver paste was deposited on the films surface to serve as electrodes. The measurements were carried out in the temperature range of 25–300 °C in air. Total conductivity of the LLZ films was calculated taking into account the thickness and electrode area of the measured samples.

### 3. Results and Discussion

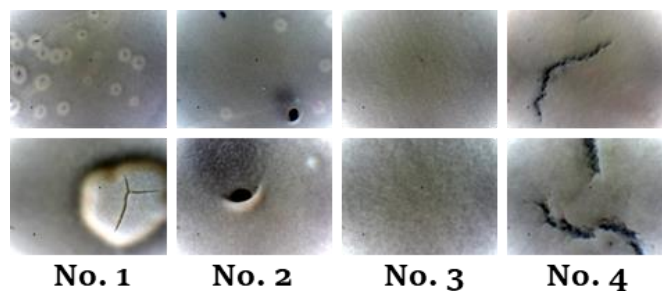
LLZ powder with tetragonal modification was obtained by sol-gel method. According to XRD analysis the compound was single-phase, Figure 1. The average grain size of the obtained powder (3–5 μm) was previously estimated by laser-diffraction particle size analyzer [26]. The slurry composition was chosen with a minimum content of organic components.

The solvent and dispersant contents were fixed at 60 and 1 wt.%, respectively (Table 1). In the first composition, the solid electrolyte LLZ was taken in the amount of 30 wt.%. The binder/plasticizer ratio was 2:1. All compositions were obtained under the same conditions. The slurry compositions with different amounts of organic components are presented in Table 1.

The LLZ films surfaces with different composition deposited on Ni substrate are shown in Figure 1. It can be seen that composition No. 1 has a large number of defects in the form of small pores. Increasing the binder content to 7 wt.% leads to pore growth, which has a negative effect on the thin-film surface. According to the literature [27], the presence of pores is probably caused by an increase in slurry viscosity. The increase in viscosity lead to difficulty in gas removal from the film volume. On the other hand, the binder amount reduction to 5 wt.% leads to the homogeneous surface formation, without any defects. The cracks formation of LLZ film is caused by further reduction of the binder amount to 4 wt.%. In the literature [27], this defect is called Crow's-Foot Cracking, which occurs due to the lateral shrinkage stress increase because of binder and plasticizer deficit. Therefore, the composition No. 3 is the optimal slurry composition for the LLZ film casting and further research.

**Table 1** Compositions of LLZ slurry for tape casting.

Component	Composition (wt.%)			
	No. 1	No. 2	No. 3	No. 4
Li <sub>7</sub> La <sub>3</sub> Zr <sub>2</sub> O <sub>12</sub>	30	28.5	31.5	33
Polyvinyl Butyral (PVB)	6	7	5	4
Polyethylene Glycol (PEG)	3	3.5	2.5	2
Fish oil	1	1	1	1
Isopropanol	60	60	60	60



**Figure 1** Surface of the dried LLZ coatings obtained by tape casting on Ni substrate.

The temperature mode for organic components removal was chosen based on differential scanning calorimetry (DSC) data. According to the DSC data (Figure 2), the volatilization of H<sub>2</sub>O, CO, CO<sub>2</sub> occurs in the temperature range from 100 to 500 °C. The most intense volatilization of gases was observed in the range from 300 to 400 °C. An additional exothermic peak in the range from 700 to 800 °C is observed on the CO<sub>2</sub> mass spectrum, which indicates the presence of remaining carbon in the film after annealing at 500 °C. This is also confirmed by mass change: the first mass loss begins at ~110 °C, the second at ~320 °C and the third at ~710 °C. PEG begins to decompose at ~360 °C, and thermolysis of PVB starts in the temperature range of 180–200 °C (GOST 9439-85 [28]).

Optical dilatometry was used to choose the heating rate for the LLZ solid electrolyte films' annealing. According to the obtained data, heating with 5 °C·min<sup>-1</sup> rate led to the significant film deformation at the initial stages of heating. At the same time, at a heating rate of 2 °C·min<sup>-1</sup> from 25 to 200 °C, an increase in the observed size of the film occurs, forming an uneven profile of the film along its length, which indicates deformation of the film (Figure 3). Minor deformations are observed up to 400 °C; upon further heating, the volume of the sample first decreases and then practically does not change. Thus, volumetric changes in the film are associated with the removal of organic components, which is in good agreement with the DSC data.

Thus, based on the obtained results, an optimal three-stage heat treatment mode for the organic components removal was proposed:

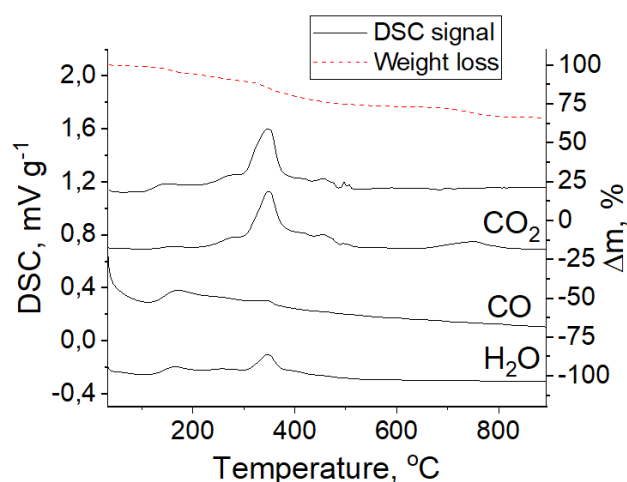
1) heating from 25 to 200 °C (2 °C·min<sup>-1</sup>) and exposure at 200 °C for 1 h;

2) heating from 200 to 500 °C (5 °C·min<sup>-1</sup>) and exposure at 500 °C for 30 min;

3) heating from 500 °C to the final annealing temperature of 600, 700, 800 or 900 °C (5 °C·min<sup>-1</sup>) and exposure for 30 min.

According to the XRD data, in the temperature range of 600–700 °C, the phase transition of LLZ from tetragonal to cubic modification is observed (Figure 4). The presence of this phase transition was confirmed by high-temperature XRD of the initial LLZ powder with tetragonal structure in work [16]. The films consist of a well-formed cubic LLZ phase after annealing above 600 °C. However, an impurity phase of lanthanum zirconate appears after film annealing

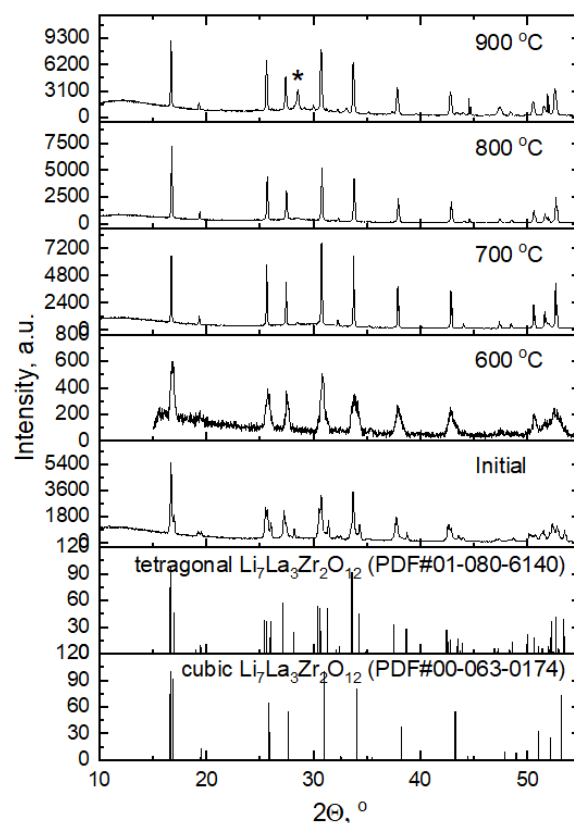
at 900 °C, which is associated with the evaporation of lithium oxide [21].



**Figure 2** DSC and TG curves for LLZ film.



**Figure 3** Optical micrographs of LLZ film during heating (2 °C min<sup>-1</sup>).

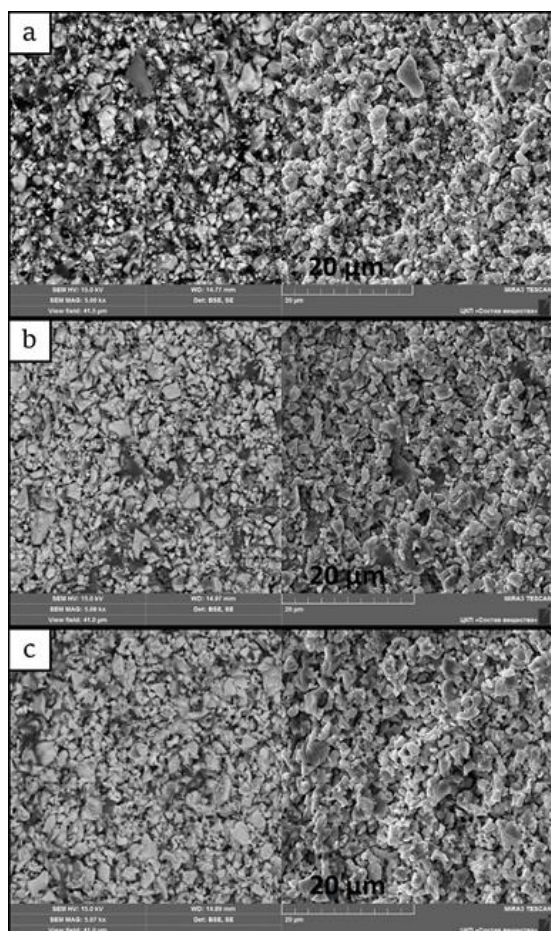


**Figure 4** XRD patterns of LLZ films annealed at different temperatures. \* - La<sub>2</sub>Zr<sub>2</sub>O<sub>7</sub> (PDF#01-071-2363).

The morphology and size of ceramic grains of thin-film electrolytes based on  $\text{Li}_7\text{La}_3\text{Zr}_2\text{O}_{12}$  obtained by tape casting and annealed at temperatures of 600, 700 and 800 °C were studied using SEM. Figure 5 shows micrographs of the studied films; they have a quite developed surface, which can lead to improved contact with the electrode material and an increase in the reaction zone area. The average grain size of LLZ films after heat treatment does not change significantly (1–5  $\mu\text{m}$ ), and it is in good agreement with the grains size of the initial LLZ powder [26].

The LLZ films' surface after the heat treatment at 600, 700 and 800 °C was investigated by elemental analysis. According to the obtained data, the solid electrolytes have a uniform distribution of elements in the structure. Neither impurity phases nor interaction products with the Ni substrate were detected. However, the presence of a carbon-containing phase can be observed for LLZ films annealed at 600 °C, Figure 6. This product may indicate an incomplete organic additive removal process. No traces of this phase were found for LLZ films annealed at 700 and 800 °C.

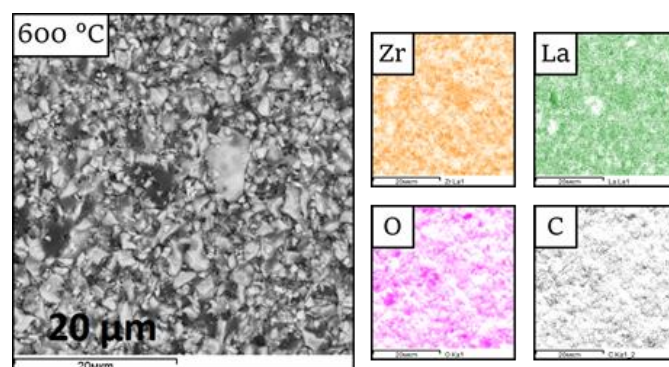
The cross-sections of the LLZ solid electrolyte films before and after annealing at different temperatures are shown in Figure 7. The obtained films have a uniform coating over the whole section, without any defects. The thickness of the initial film was equal to  $\sim 35 \mu\text{m}$ , Figure 7a. After annealing at 600 °C, the film thickness decreased to  $\sim 23 \mu\text{m}$  and did not change subsequently.



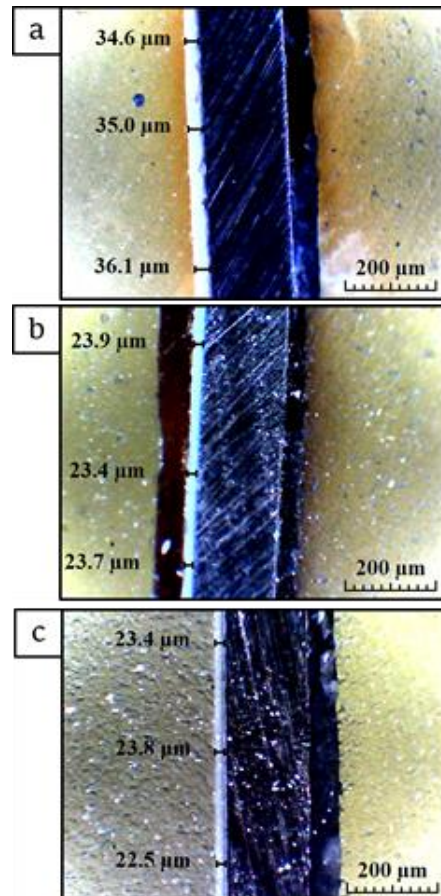
**Figure 5** SEM micrographs of the LLZ films annealed at 600 °C (a); 700 °C (b); 800 °C (c).

The densities of the obtained samples were determined by hydrostatic weighing. The annealed samples were weighed in gasoline with the density of  $0.7 \text{ g}\cdot\text{cm}^{-3}$ . The relative densities were 65 and 68 wt.% for the samples annealed at 700 and 800 °C, respectively.

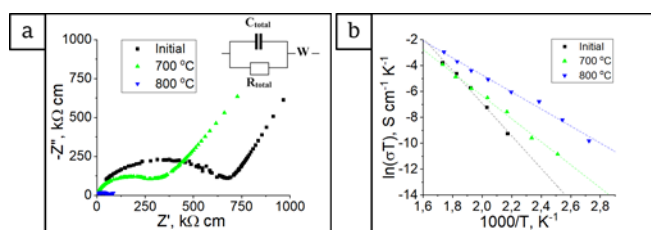
The initial and annealed ceramic membranes were examined by impedance spectroscopy. The typical impedance plots at 215 °C for LLZ films are shown in Figure 8a. The impedance plots have only one semicircle, which is starting from zero. It was not possible to separate the contributions of bulk and grain-boundary resistances. The similar type of impedance plots was observed in other works [29–31], and the obtained semicircle refers to the total resistance of the solid electrolyte.



**Figure 6** SEM micrograph of the LLZ film annealed at 600 °C (a) and element distribution maps for oxygen, zirconium, lanthanum, and carbon.



**Figure 7** Optical micrographs of the cross-sections of LLZ films: initial (a); annealed at 600 °C (b) and 800 °C (c).



**Figure 8** Impedance plots at 215 °C (a) and Arrhenius plot for the total conductivity of initial and annealed LLZ films (b).

The temperature dependences of total conductivity of LLZ films annealed at different temperatures are linear in the studied temperature range, Figure 8b. The total conductivity growth of LLZ films after their heat treatment can be observed. This effect can be caused by the complete removal of organic components and sintering of ceramic membranes. The values of total conductivity at different temperatures and activation energy of the conductivity for the studied samples are given in Table 2. It can be seen that the activation energy values of the dried LLZ film are significantly higher compared to LLZ films annealed at 700 and 800 °C. As it was mentioned above the annealing at 700 °C leads to the removing of organic components, which does not have lithium-ion conductivity. Then the annealing temperature increase from 700 to 800 °C leads to the samples' densification, which, in turn, leads to the increase in the conductivity of the samples and facilitating of lithium-ion transport. The film annealed at 800 °C has the conductivity value of  $6.6 \cdot 10^{-9} \text{ S} \cdot \text{cm}^{-1}$  at room temperature. However, the total conductivity of LLZ bulk samples with tetragonal structure is equal to  $\sim 10^{-7} \text{ S} \cdot \text{cm}^{-1}$  at room temperature [21, 26]. Thus, LLZ solid electrolyte films formed by tape casting and annealed at 800 °C has underestimated values of lithium-ion conductivity compared to the bulk samples (pellets with a diameter of 10 mm and a thickness of 1 mm). Such difference in values of total conductivity can be caused by low density of the obtained films. This problem can be solved by introduction of some sintering additives.

#### 4. Limitations

A limitation of this study is the difficulty in interpreting impedance spectroscopy data at near room temperatures due to the high resistance values of formed by tape casting. This problem can be solved in the future by introduction of some sintering additives into LLZ or transition to high-conductive cubic modification of LLZ.

#### 5. Conclusions

Thin films of LLZ solid electrolyte with tetragonal structure were obtained by tape casting. The slurry composition has been developed for the formation of homogeneous coatings. The thickness of LLZ films after drying and annealing was equal to 35 and 23  $\mu\text{m}$ , respectively. Based on the DSC and optical dilatometry data, the optimal heat treatment mode for the obtained samples was proposed that does not lead to films' deformation. According to the XRD data, the cubic phase of LLZ without impurities was formed after films' annealing at 700 and 800 °C. Further increase in the annealing temperature leads to the formation of the additional impurity phase ( $\text{La}_2\text{Zr}_2\text{O}_7$ ). The average grain size of annealed ceramic membranes was equal to 1–5  $\mu\text{m}$ . It was established that 600 °C is not enough for the LLZ films final annealing, since there are trace amounts of organic compounds in the composition. The highest conductivity values were observed for films annealed at 800 °C –  $2.5 \cdot 10^{-7}$  and  $1.5 \cdot 10^{-5} \text{ S} \cdot \text{cm}^{-1}$  at 90 and 215 °C, respectively. Thus, the developed technique can be used to obtain LLZ films with the thickness of ceramic membranes  $\sim 30 \mu\text{m}$  by tape casting.

#### • Supplementary materials

No supplementary materials are available.

#### • Funding

This research was funded by the Research Program No. 122020100210-9 (IHTE UB RAS), Russian Academy of Sciences, Ural Branch, Russia.

#### • Acknowledgments

The research has been carried out with the equipment of the Shared Access Center “Composition of Compounds” at the IHTE UB RAS.

#### • Author contributions

Conceptualization: E.L., I.L.

Data curation: E.L., I.L., L.P.

Formal Analysis: E.L., L.P., D.K., S.B.

Funding acquisition: I.L.

Investigation: E.L., I.L., L.P., D.K., S.B.

Methodology: E.L., L.P., D.K., S.B.

Project administration: I.L.

**Table 2** Total conductivity ( $\sigma$ ) and activation energy of the conductivity ( $E_a$ ) of LLZ films annealed at different temperatures.

	Annealing temperature, °C	$E_a$ , $\text{kJ} \cdot \text{mol}^{-1}$	$\sigma$ at 25 °C, $\text{S} \cdot \text{cm}^{-1}$	$\sigma$ at 90 °C, $\text{S} \cdot \text{cm}^{-1}$	$\sigma$ at 215 °C, $\text{S} \cdot \text{cm}^{-1}$	Relative density, %
■	initial	$104.7 \pm 5.5$	$1.3 \cdot 10^{-13}$	$2.1 \cdot 10^{-10}$	$1.5 \cdot 10^{-6}$	–
▲	700	$73.9 \pm 2.4$	$3.5 \cdot 10^{-11}$	$6.0 \cdot 10^{-9}$	$3.2 \cdot 10^{-6}$	65
▼	800	$53.3 \pm 1.8$	$6.6 \cdot 10^{-9}$	$2.5 \cdot 10^{-7}$	$1.5 \cdot 10^{-5}$	68
	LLZ pellet	$56.0 \pm 1.0$	$5.6 \cdot 10^{-7}$	$2.6 \cdot 10^{-5}$	$2.3 \cdot 10^{-3}$	85

Resources: I.L.

Supervision: I.L.

Validation: E.L., I.L., L.P., D.K., S.B.

Visualization: E.L.

Writing – original draft: E.L., I.L., L.P., D.K., S.B.

Writing – review & editing: E.L., I.L.

## ● Conflict of interest

The authors declare no conflict of interest.

## ● Additional information

Author IDs:

Efim Lyalin, Scopus ID [57213417781](#);

Evgeniya Il'ina, Scopus ID [54782709600](#);

Konstantin Druzhinin, Scopus ID [35775866900](#);

Semen Belyakov, Scopus ID [56727876100](#).

Websites:

Institute of High Temperature Electrochemistry, UB RAS, <https://ihte.ru/>;

Ural Federal University, <https://urfu.ru/en/>.

## References

- Kong L, Wang L, Zhu J, Bian J, Xia W, Zhao R, Lin H, Zhao Y. Configuring solid-state batteries to power electric vehicles: A deliberation on technology, chemistry and energy. *Chem Commun.* 2021;57:12587–12594. doi:[10.1039/D1CC04368D](#)
- Bates AM, Preger Y, Torres-Castro L, Harrison KL, Harris SJ, Hewson J. Are solid-state batteries safer than lithium-ion batteries? *Joule.* 2022;6:742–55. doi:[10.1016/j.joule.2022.02.007](#)
- Wu J, Yuan L, Zhang W, Li Z, Xie X, Huang Y. Reducing the thickness of solid-state electrolyte membranes for high-energy lithium batteries. *Energy Environ Sci.* 2021;14:12–36. doi:[10.1039/D0EE02241A](#)
- Kokal I, Somer M, Notten PHL. Sol-gel synthesis and lithium ion conductivity of  $\text{Li}_7\text{La}_3\text{Zr}_2\text{O}_{12}$  with garnet-related type structure. *Solid State Ion.* 2011;185:42–46. doi:[10.1016/j.ssi.2011.01.002](#)
- Kuhn A, Narayanan S, Spencer L, Goward G. Li self-diffusion in garnet-type  $\text{Li}_7\text{La}_3\text{Zr}_2\text{O}_{12}$  as probed directly by diffusion-induced  $^7\text{Li}$  spin-lattice relaxation NMR spectroscopy. *Phys Rev B.* 2011;83:09430201. doi:[10.1103/PhysRevB.83.094302](#)
- Toda S, Ishiguro K, Shimonishi Y, Hirano A, Takeda Y, Yamamoto O, Imanishi N. Low temperature cubic garnet-type  $\text{CO}_2$ -doped  $\text{Li}_7\text{La}_3\text{Zr}_2\text{O}_{12}$ . *Solid State Ion.* 2013;233:102–106. doi:[10.1016/j.ssi.2012.12.007](#)
- Larraz G, Orera A, Sanjuan ML. Cubic phases of garnet type  $\text{Li}_7\text{La}_3\text{Zr}_2\text{O}_{12}$ : The role of hydration. *J Mater Chem A.* 2013;1:11419–11428. doi:[10.1039/C3TA11996C](#)
- Xie H, Li Y, Goodenough JB. Low-temperature synthesis of  $\text{Li}_7\text{La}_3\text{Zr}_2\text{O}_{12}$  with cubic garnet-type structure. *Mater Res Bull.* 2012;47:1229–1232. doi:[10.1016/j.materresbull.2012.01.027](#)
- Campanella D, Belanger D, Paoletta A. Beyond garnets, phosphates and phosphosulfides solid electrolytes: New ceramic perspectives for all solid lithium metal batteries. *J Power Source.* 2021;482:228949. doi:[10.1016/j.jpowsour.2020.228949](#)
- Zheng F, Kotobuki M, Song S, Lai MO, Lu L. Review on solid electrolytes for all-solid-state lithium-ion batteries. *J Power Source.* 2018;389:198–213. doi:[10.1016/j.jpowsour.2018.04.022](#)
- Yaroslavtsev AB. Solid electrolytes: Main prospects of research and development. *Rus Chem Rev.* 2016;85:1255–1276. doi:[10.1070/RCR4634](#)
- Dunushkina LA. Introduction to methods of obtaining film electrolytes for solid oxide fuel cells: monograph. Yekaterinburg: UrB RAS; 2015. 128 p. Russian.
- Tan J, Tiwari A. Fabrication and characterization of  $\text{Li}_7\text{La}_3\text{Zr}_2\text{O}_{12}$  thin films for lithium ion battery. *ECS Solid State Lett.* 2012;1(6):57. doi:[10.1149/2.013206ssl](#)
- Tadanaga K, Egawa H, Hayashi A, Tatsumisago M, Mosa J, Aparicio M, Duran A. Preparation of lithium ion conductive Al-doped  $\text{Li}_7\text{La}_3\text{Zr}_2\text{O}_{12}$  thin films by a sol-gel process. *J Power Sources.* 2015;273:844–847. doi:[10.1016/j.jpowsour.2014.09.164](#)
- Bitzer M, Gestel TV, Uhlenbruck S, Buchkremer PH. Sol-gel synthesis of thin solid  $\text{Li}_7\text{La}_3\text{Zr}_2\text{O}_{12}$  electrolyte films for Li-ion batteries. *Thin Solid Films.* 2016;615:128–134. doi:[10.1016/j.tsf.2016.07.010](#)
- Lyalin E, Il'ina E, Kalinina E, Antonov B, Pankratov A, Pereverzev D. Electrophoretic deposition and characterization of thin-film membranes  $\text{Li}_7\text{La}_3\text{Zr}_2\text{O}_{12}$ . *Membranes.* 2023;13(5):468. doi:[10.3390/membranes13050468](#)
- Yi E, Wang W, Kieffer J, Richard M, Key L. Parameters governing the densification of cubic- $\text{Li}_7\text{La}_3\text{Zr}_2\text{O}_{12}$   $\text{Li}^+$  conductors. *J Power Sources.* 2017;352:156–164. doi:[10.1016/j.jpowsour.2017.03.126](#)
- Hanc E, Zajac W, Lu L, Binggong Y, Kotobuki M, Ziabka M, Molenda J. On fabrication procedures of Li-ion conducting garnets. *J Solid State Chem.* 2017;248:51–60. doi:[10.1016/j.jssc.2017.01.017](#)
- Hitz GT, Dennis W. McOwen, Zhang L, Ma Z, Fu Z, Wen Y, Gong Y, Dai J, Tanner RH, Hu L, Wachsmas ED. High-rate lithium cycling in a scalable trilayer Li-garnet-electrolyte architecture. *Mater Today.* 2019;22:50–57. doi:[10.1016/j.mattod.2018.04.004](#)
- Ye R, Tsai CL, Ihrig M, Sevinc S, Rosen M, Dashjav E, Sohn YJ, Figgemeier E, Finsterbusch M. Water-based fabrication of garnet-based solid electrolyte separators for solid-state lithium batteries. *Green Chem.* 2020;22(15):4952–4961. doi:[10.1039/d0gc01009j](#)
- Ramakumar S, Deviannapoorani C, Dhivya L, Shankar LS, Murugan R. Lithium garnets: Synthesis, structure,  $\text{Li}^+$  conductivity,  $\text{Li}^+$  dynamics and applications. *Prog Mater Sci.* 2017;88: 325–411. doi:[10.1016/j.pmatsci.2017.04.007](#)
- Meshcherskikh AN, Khaliullina ASH, Dunyushkina LA, inventors; Private Institution for the scientific development of the nuclear industry "Science and Innovation", assignee. The composition of the slurry for the production of porous ceramics. Russian Federation patent RU 2021139410. 2021 Dec 12. Russian.
- Murugan R, Thangadurai V, Weppner W, Angew. Fast lithium ion conduction in garnet-type  $\text{Li}_7\text{La}_3\text{Zr}_2\text{O}_{12}$ . *Chem Int Ed.* 2007;46:7778–7781. doi:[10.1002/anie.200701144](#)
- Kotobuki M, Munakata H, Kanamura K, Sato Y, Yoshida T. Compatibility of  $\text{Li}_7\text{La}_3\text{Zr}_2\text{O}_{12}$  solid electrolyte to all-solid-state battery using Li metal anode. *J Electrochem Soc.* 2010;157:1076–1079. doi:[10.1149/1.3474232](#)
- Awaka J, Kijima N, Hayakawa H, Akimoto J. Synthesis and structure analysis of tetragonal  $\text{Li}_7\text{La}_3\text{Zr}_2\text{O}_{12}$  with the garnet-related type structure. *J Solid State Chem.* 2009;182:2046–2052. doi:[10.1016/j.jssc.2009.05.020](#)
- Il'ina EA, Andreev OL, Antonov BD, Batalov NN. Morphology and transport properties of the solid electrolyte  $\text{Li}_7\text{La}_3\text{Zr}_2\text{O}_{12}$  prepared by the solid-state and citrate-nitrate methods. *J Power Sources.* 2012;201:169–173. doi:[10.1016/j.jpowsour.2011.10.108](#)
- Richard EM, Eric RT. *Tape Casting: Theory and Practice.* Wiley. 2000. 298 p.
- GOST 9439-85 Polyvinyl Butyral. Technical conditions. – Moscow: Publishing House of Standards. 1985. 38 p.

29. Lazanas AC, Prodromidis MI. Electrochemical Impedance Spectroscopy - A Tutorial. ACS Measurement Science Au. 2023;3:162–193. doi:[10.1021/acsmeasuresciau.2c00070](https://doi.org/10.1021/acsmeasuresciau.2c00070)
30. Shen H, Yi E, Heywood S, Parkinson DY, Chen G, Tamura N, et al. Scalable freeze-tape-casting fabrication and pore structure analysis of 3D LLZO solid-state electrolytes. ACS Appl Mater Interfaces. 2019;12:3494–3501. doi:[10.1021/acsami.9b11780](https://doi.org/10.1021/acsami.9b11780)
31. Fu Z, Zhang L, Gritton JE, Godbey G, Hamann T, Gong Y, et al. Probing the mechanical properties of a doped  $\text{Li}_7\text{La}_3\text{Zr}_2\text{O}_{12}$  garnet thin electrolyte for solid-state batteries. ACS Appl Mater Interfaces. 2020;12:24693–24700. doi:[10.1021/acsami.0c01681](https://doi.org/10.1021/acsami.0c01681)